Dynamic FEM simulation of wheel-rail rolling contact with friction in an Eulerian frame - Application to curve squeal

Van-Vuong Lai, Olivier Chiello, Jean-François Brunel, Philippe Dufrenoy

Dynamic FEM simulation of wheel-rail rolling contact with friction in an Eulerian frame - Application to curve squeal

V-V Lai [1,2], **O.Chiello** [2], **J.-F.Brunel** [1], **P.Dufrénoy** [1]
[1] Univ. Lille, CNRS, Centrale Lille, FRE 2016 - LaMcube -
Laboratoire de Mécanique Multiphysique Multiéchelle, F-59000, Lille, France
[2] Univ Lyon, IFSTTAR, CEREMA, UMRAE, F-69675, Lyon, France
e-mail: **van-vuong.lai@polytech-lille.fr, olivier.chiello@ifsttar.fr**

Abstract
The aim of this paper is to develop a full Finite Element (FE) computational method for the dynamics of wheel/rail frictional rolling contact systems in order to calculate reference solutions in curve squeal. The proposed method is characterized by the use of a fine FE discretization of the contact surface in an Eulerian frame, non-smooth frictional contact laws and model reduction techniques. An application to the wheel/rail frictional rolling contact is presented in both quasi-static and dynamic cases. The validation of the approach in quasi-static conditions is carried out by comparison with CONTACT software. Stability and transient results show that the technique is able to simulate friction-induced vibrations at high frequencies.

1 Introduction

In the case of a tight radius curve, squeal can be generated due to the unstable slip of the wheel on the head of the rail. The mechanism causing the instability is however still controversial. A negative slope of the friction coefficient depending on creepage velocity is introduced in some models as a source of the instability whereas squeal can also occur in the case of constant friction due to mode coupling instability in other models.

There are actually wheel/rail rolling contact models with some simplifications. Equivalent point-contact models are based on analytic formulas or heuristic laws of frictional rolling contact [1, 2]. They give good results in slightly non linear dynamic cases close to pure rolling [3]. However, in the cases of large slips and high-frequency dynamics, surface contact models are more adapted. They need a discretization of the contact zone. The variational theory of Kalker [2] which is used in Pieringer's model [4] performs some simplifications as the semi-analytical computation of the local contact flexibilities or influence functions (Boussinesq and Cerruti elastic half-space assumptions, contact/friction decoupling). In the case of friction-induced vibrations in curves characterized by large slips, high frequency dynamics and very fast evolutions in the contact zone, the impact of these simplifications is unknown.

Finite element wheel/rail frictional rolling contact models use commercial softwares [5, 6] but the calculation is generally performed in a Lagrangian reference frame, which greatly limits its performance and is not adapted to high frequency dynamics.

The aim of the paper is to propose a full finite Element method for modeling friction induced vibration of the wheel-rail contact in curves. The wheel-rail contact is simulated by surface contact models with a discretization of the contact zone and non-smooth frictional contact laws. To reduce computational costs, simulations are performed in a Eulerian reference frame and modal reduction strategies are used. Instabilities are analyzed through 2 types of analysis: stability analysis to predict unstable modes assuming a full steady steading in the contact zone, and a transient analysis which allows to introduce non linearities

ans to determine amplitude of vibrations. By using finite element method, discretization of the contact surface, non-smooth frictional contact laws and model reduction techniques in an Eulerian frame. Reduction base including free-interface modes and static attachment modes is used to reduce computing duration. The proposed approach is applied for contact between the rail and the wheel during curving.

2 Finite Element (FE) formulation in the time-domain

2.1 Contact problem in the Eulerian frame

A wheel/rail rolling contact is considered, as shown in Fig. 1. The $z-$axis is chosen to coincide with the common normal to the two surfaces in contact, the longitudinal $x-$axis corresponds to the rolling direction and the $y-$axis refers to the lateral direction. The wheel rolling speed is V in a direction parallel to $x-$axis . In case of curving, wheel relative lateral velocities ΔV_y and longitudinal velocities ΔV_x have to be considered. The wheel may also have a relative angular velocity $\Delta\omega_z$ around their common normal (or spin).

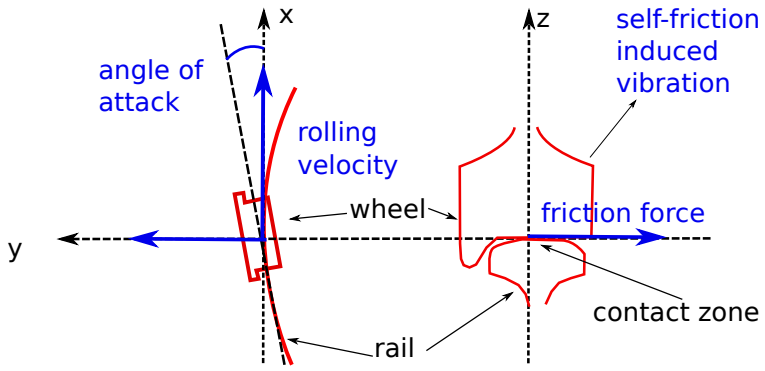

Figure 1: Coordinate system, kinetic variables and applied forces

According to [7], in the Eulerian frame which moves with the point of contact, the relative sliding instantaneous velocities (or creep velocities) between the wheel and the rail at a fixed point of the potential contact interface are given by:

$$\begin{aligned} \dot{s}_x &= v_x^W - v_x^R = \Delta V_x - \Delta\omega_z y + V(\frac{\partial u_x^W}{\partial x} - \frac{\partial u_x^R}{\partial x}) + (\dot{u}_x^W - \dot{u}_x^R) \\ \dot{s}_y &= v_y^W - v_y^R = \Delta V_y + \Delta\omega_z x + V(\frac{\partial u_y^W}{\partial x} - \frac{\partial u_y^R}{\partial x}) + (\dot{u}_y^W - \dot{u}_y^R) \end{aligned} \tag{1}$$

where R, W denote respectively the rail and the wheel. $\mathbf{u}(x, y, z, t)$ and $\mathbf{v}(x, y, z, t)$ denote respectively the displacement and velocity fields of the structure in the Eulerian frame and the notation $\dot{u} = \frac{\partial u}{\partial t}$ refers to the time partial derivative. The terms involving $V\frac{\partial u}{\partial x}$ represent the deformation contributions due to rolling in the Eulerian frame whereas the terms involving $\dot{u}$ simply represent the dynamic contributions.

2.2 Contact laws

To deal with unilateral contact on the interface, a non-regularized Signorini law is chosen:

$$\begin{aligned} \Delta u_n - g &\leq 0 \\ r_n &\leq 0 \\ (\Delta u_n - g) r_n &= 0 \end{aligned} \tag{2}$$

where $\Delta u_n = u_n^W - u_n^R$ is the normal relative displacement on the potential contact interface, r_n is the normal contact stress and g is the initial gap. This law simply conveys that (i) there is no interpenetration between the two bodies, (ii) the interface only undergoes compression and (iii) it respects the condition of complementarity. A equivalent semi-regularized form of the law uses the projection on the negative real set (cf. for instance [8]):

$$r_n = \text{Proj}_{\mathbb{R}^-}\left(r_n - \rho_n \Delta u_n\right) \qquad \forall \rho_n > 0 \tag{3}$$

where $\text{Proj}_{\mathbb{R}^-}(x) = \min(x, 0)$ and ρ_n is a positive real number called normal augmentation parameter.

To deal with frictional contact, a non-regularized Coulomb law with a constant friction coefficient μ is used:

$$\begin{aligned} \|\mathbf{r}_t\| &\leq -\mu r_n \\ \|\mathbf{r}_t\| = -\mu r_n &\Rightarrow \exists \lambda > 0,\ \dot{\mathbf{s}}_\mathbf{t} = -\lambda \mathbf{r}_t \\ \|\mathbf{r}_t\| < -\mu r_n &\Rightarrow \dot{\mathbf{s}}_\mathbf{t} = 0 \end{aligned} \tag{4}$$

where $\dot{\mathbf{s}}_\mathbf{t}$ is the vectorial creep velocity with components $\dot{s}_x$ and $\dot{s}_y$ defined in equation (1) and $\mathbf{r}_t$ is the tangential stress due to friction. This law states that the frictional reaction cannot be greater than a limit $-\mu r_n$. If the limit is reached, the material particle slides and has a direction opposed to the direction of the reaction (slip state). In other cases, the relative velocity is null (stick state).

A equivalent semi-regularized form of the law uses the projection on the Coulomb cone (cf. for instance [8]):

$$\mathbf{r}_t = Proj_{\mathcal{C}}\left(\mathbf{r}_t - \rho_t \dot{\mathbf{s}}_\mathbf{t}\right) \qquad \forall \rho_t > 0 \tag{5}$$

where $Proj_{\mathcal{C}}(\mathbf{x}) = \min(\frac{\mu|r_n|}{\|\mathbf{x}\|}, 1)\mathbf{x}$ and ρ_t is a positive real number called tangential augmentation parameter.

2.3 Dynamics equations and FE discretization

Convective terms in the equations of motion induced by the Eulerian frame are only significant in the case where the rotational speed is in the order of magnitude of the eigenfrequencies ([9]). In the following application, the effects of the convective terms are neglected because the wheel rotational speed is assumed low in comparison to the wheel/rail eigenfrequencies.

The displacement field $\mathbf{u}$ must verify the equations of continuum mechanics [10] together with the local formulations of contact equations Eqs. (3) and (5). In order to introduce FE approximations, the principle of virtual power is used for the system dynamics and the contact laws are written in weak forms [11]:

$$\begin{gathered} \text{Find } \mathbf{u} \in \mathcal{U} \text{ and } \mathbf{r} \text{ such as } \forall \mathbf{u}^* \in \mathcal{U}^o \text{ and } \forall \mathbf{r}^* \\ \int_\Omega \rho \mathbf{u}^*.\ddot{\mathbf{u}} d\Omega + \int_\Omega \epsilon(\mathbf{u}^*) : \sigma(\mathbf{u}) d\Omega = \int_\Omega \mathbf{u}^*.\mathbf{f}_s d\Omega + \int_{\partial\Omega_F} \mathbf{u}^*.\mathbf{f}_d ds + \int_{S_c} \mathbf{u}^*.\mathbf{r} ds \\ \int_{S_c} r_n^* r_n ds = \int_{S_c} r_n^* \text{Proj}_{\mathbb{R}^-}\left(r_n - \rho_n \Delta u_n\right) ds \\ \int_{S_c} \mathbf{r}_t^* \mathbf{r}_t ds = \int_{S_c} \mathbf{r}_t^* \text{Proj}_C\left(\mathbf{r}_t - \rho_t \dot{\mathbf{s}}_\mathbf{t}\right) ds \end{gathered} \tag{6}$$

where Ω is the whole structure. $\mathbf{f_s}$ and $\mathbf{f_d}$ are respectively a volume load in Ω and a surface load on a surface $\delta\Omega_F$.$\epsilon(\mathbf{u})$ and $\sigma(\mathbf{u})$ stand respectively for the symmetric gradient and the stress tensor corresponding to any displacement field $\mathbf{u}$, the notation $\ddot{\mathbf{u}} = \frac{\partial^2 \mathbf{u}}{\partial t^2}$ refers to the double time partial derivative, $\mathcal{U} = \{\mathbf{u} | \mathbf{u} = \mathbf{u}_d \text{ on } \partial\Omega_u\}$ and $\mathcal{U}^0 = \{\mathbf{u} | \mathbf{u} = \mathbf{0} \text{ on } \partial\Omega_u\}$. $\delta\Omega_u$ is the part of the boundary of the domain Ω where a displacement $\mathbf{u_d}$ is prescribed on. S_c is the potential contact zone.

By using appropriate shape interpolation functions for unknown and test displacement and reaction fields $(\mathbf{u}, \mathbf{r}, \mathbf{u}^*, \mathbf{r}^*)$, finite element discretization of Eq. (6) directly gives:

$$\begin{aligned} \mathbf{M}\ddot{\mathbf{U}} + \mathbf{C}\dot{\mathbf{U}} + \mathbf{K}\mathbf{U} &= \mathbf{F} + {\mathbf{P_n}}^T\mathbf{R_n} + {\mathbf{P_t}}^T\mathbf{R_t} \\ \mathbf{R_n} &= \int_{S_c} {\mathbf{N_n}}^T \text{Proj}_{\mathbb{R}^-}(\mathbf{N_n}(\mathbf{H_n^{-1}}\mathbf{R_n} - \rho_n(\mathbf{P_n}\mathbf{U} - \mathbf{G}))ds \\ \mathbf{R_t} &= \int_{S_c} {\mathbf{N_t}}^T \text{Proj}_{\mathcal{C}}(\mathbf{N_t}(\mathbf{H_t^{-1}}\mathbf{R_t} - \rho_t\dot{\mathbf{S}}_\mathbf{t}(\mathbf{P_t}\mathbf{U}, \mathbf{P_t}\dot{\mathbf{U}})))ds \end{aligned} \tag{7}$$

where $\mathbf{U}$, $\mathbf{R_n}$ and $\mathbf{R_t}$ denote respectively the vectors of nodal displacements, equivalent normal reactions and equivalent friction forces, $\mathbf{M}, \mathbf{C}, \mathbf{K}$ are respectively the mass, damping and stiffness matrices of the structure without contact, $\mathbf{G}$ is the vector of nodal initial gaps and $\mathbf{N_n}, \mathbf{N_t}$ are the shape function vectors on the contact interface. In addition, $\mathbf{P_n}, \mathbf{P_n}$ are matrices allowing to pass the contact reactions from the local relative frame to the global frame whereas $\mathbf{H_n} = \int_{S_c} {\mathbf{N_n}}^T\mathbf{N_n}ds$ and $\mathbf{H_t} = \int_{S_c} {\mathbf{N_t}}^T\mathbf{N_t}ds$ are transformation matrices from nodal to equivalent forces. Finally, $\dot{\mathbf{S}}_\mathbf{t}(\mathbf{P_t}\mathbf{U}, \mathbf{P_t}\dot{\mathbf{U}})$ denotes the vector of nodal creep velocities which can be determined linearly from local displacement and velocity vectors, taking into account quasi-static creep velocities (cf. Eq. (1)).

3 Reduction strategies

The principle is to search an approximated solution $\mathbf{U} = \mathbf{B}\mathbf{q_r}$ of the problem spanned by a reduced basis $\mathbf{B}$ which leads to a reduced dynamics equation:

$$\mathbf{M_r}\ddot{\mathbf{q}}_\mathbf{r} + \mathbf{C_r}\dot{\mathbf{q}}_\mathbf{r} + \mathbf{K_r}\mathbf{q_r} = \mathbf{B}^T(\mathbf{F} + {\mathbf{P_n}}^T\mathbf{R_n} + {\mathbf{P_t}}^T\mathbf{R_t}) \tag{8}$$

where $\mathbf{M_r}, \mathbf{C_r}, \mathbf{K_r} = \mathbf{B}^T(\mathbf{M_r}, \mathbf{C_r}, \mathbf{K_r})\mathbf{B}$ and the size of the system is reduced to the number of modes in basis $\mathbf{B}$.

In this paper, the proposed basis B includes free-interface normal modes of the structure and static attachment modes $\mathbf{B} = [\Phi \quad \Phi_s]$. Matrix Φ contains the real solutions of the free and undamped system:

$$(\mathbf{K} - \omega^2\mathbf{M})\mathbf{U} = \mathbf{0} \tag{9}$$

whereas Φ_s make the base statically complete by adding static solutions to unitary forces (normal and tangential) on the contact interface:

$$\mathbf{K}\Phi_s = {\mathbf{P_c}}^T \tag{10}$$

An approximation consists in neglecting the dynamic terms in the reduced equations corresponding to attachment modes. However, bases Φ and Φ_s are not orthogonal which is a necessary condition in order to separate the contributions of normal modes and attachments modes. This can be fixed by using residual attachment modes defined by:

$$\tilde{\Phi}_s = \Phi_s - \Phi(\Phi^T\mathbf{K}\Phi)^{-1}\Phi^T{\mathbf{P_c}}^T \tag{11}$$

These modes are the static displacement responses to unit contact reactions after the elimination of the contribution of normal modes. It can be easily verified that $\tilde{\Phi}_s^T\mathbf{K}\Phi = \mathbf{0}$.

The use of basis $\mathbf{B} = [\Phi \quad \tilde{\Phi}_s]$ in Eq. (8) together with the elimination of the dynamic terms relating to attachments modes gives:

$$\begin{aligned} \Phi^T\mathbf{M}\Phi\ddot{\mathbf{q}} + \Phi^T\mathbf{C}\Phi\dot{\mathbf{q}} + \Phi^T\mathbf{K}\Phi\mathbf{q} &= \Phi^T(\mathbf{F} + {\mathbf{P_n}}^T\mathbf{R_n} + {\mathbf{P_t}}^T\mathbf{R_t}) \\ \tilde{\Phi}_s^T\mathbf{K}\tilde{\Phi}_s\mathbf{q_s} &= \tilde{\Phi}_s^T(\mathbf{F} + {\mathbf{P_n}}^T\mathbf{R_n} + {\mathbf{P_t}}^T\mathbf{R_t}) \end{aligned} \tag{12}$$

where $\mathbf{q}$ and $\mathbf{q_s}$ are the generalized coordinate vectors corresponding respectively to normal modes and residual attachment modes such that $\mathbf{U} = \Phi\mathbf{q} + \tilde{\Phi}_s\mathbf{q_s}$. A total decoupling between the generalized equations corresponding to free-interface normal modes and residual static attachment modes is obtained.

In addition, noticing that:

$$\begin{aligned}\tilde{\Phi}_s^T \mathbf{K} \tilde{\Phi}_s \mathbf{q_s} &= (\Phi_s^T - \mathbf{P_c}\Phi(\Phi^T\mathbf{K}\Phi)^{-1}\Phi^T)\mathbf{K}(\Phi_s - \Phi(\Phi^T\mathbf{K}\Phi)^{-1}\Phi^T{\mathbf{P_c}}^T)\mathbf{q_s} \\ &= (\mathbf{P_c}\Phi_s - \mathbf{P_c}\Phi(\Phi^T\mathbf{K}\Phi)^{-1}\Phi^T{\mathbf{P_c}}^T)\mathbf{q_s} \\ &= \mathbf{P_c}\tilde{\Phi}_s\mathbf{q_s} \\ &= \mathbf{P_c}(\mathbf{U} - \Phi\mathbf{q})\end{aligned} \tag{13}$$

and including the above expression in Eq. (8) gives:

$$\begin{aligned}\Phi^T\mathbf{M}\Phi\ddot{\mathbf{q}} + \Phi^T\mathbf{C}\Phi\dot{\mathbf{q}} + \Phi^T\mathbf{K}\Phi\mathbf{q} &= \Phi^T(\mathbf{F} + {\mathbf{P_n}}^T\mathbf{R_n} + {\mathbf{P_t}}^T\mathbf{R_t}) \\ \mathbf{P_c}\mathbf{U} &= \tilde{\Phi}_s^T(\mathbf{F} + {\mathbf{P_n}}^T\mathbf{R_n} + {\mathbf{P_t}}^T\mathbf{R_t}) + \mathbf{P_c}\Phi\mathbf{q}\end{aligned} \tag{14}$$

It must be emphasized that, with this formulation, contact displacements $\mathbf{P_c}\mathbf{U}$ can be directly calculated from expanded forces and normal modes coordinates.

This reduction strategy consists in solving the global dynamics using free-interface normal modes and adding a local static residual flexibility controlled by matrix $\tilde{\Phi}_s^T$ in the expression of the contact displacements. This method gets very close to models such Pieringer's one [4] combining modal dynamics and static local resolutions of the kind of CONTACT software. However, in the proposed method, the local flexibility is calculated numerically by finite elements instead of using semi-analytical influence functions derived from Boussinesq's approximations. In addition, it takes into account the static normal/tangential coupling in the contact zone.

4 Stability analysis

The aim of the stability analysis is to address the mechanism of curve squeal due to frictional contact through the determination of the evolution of small perturbations around the steady sliding equilibrium.

4.1 Quasi-static equilibrium

The quasi-static or steady sliding equilibrium is first obtained by neglecting the dynamic terms in Eqs. (1) and (7):

$$\begin{aligned}\mathbf{K}\mathbf{U^e} &= \mathbf{F} + \mathbf{P_n^T}\mathbf{R_n^e} + \mathbf{P_t^T}\mathbf{R_t^e} \\ \mathbf{R_n^e} &= \int_{S_c} \mathbf{N_n^T}\mathrm{Proj}_{\mathbb{R}^-}(\mathbf{N_n}(\mathbf{H_n^{-1}}\mathbf{R_n^e} - \rho_n(\mathbf{P_n}\mathbf{U^e} - \mathbf{G})))ds \\ \mathbf{R_t^e} &= \int_{S_c} \mathbf{N_t^T}\mathrm{Proj}_{\mathcal{C}}(\mathbf{N_t}(\mathbf{H_t^{-1}}\mathbf{R_t} - \rho_t\dot{\mathbf{S}}_\mathbf{t}^\mathbf{e})ds\end{aligned} \tag{15}$$

where $\dot{\mathbf{S}}_\mathbf{t}^\mathbf{e} = \dot{\mathbf{S}}_\mathbf{t}(\mathbf{P_t}\mathbf{U^e}, \mathbf{0})$ is the vector of nodal quasi-static creepage velocities.

Assuming that some solutions of Eq. (15) exist and can be calculated, it notably provides the status of the nodes on the contact interface as a function of the equivalent normal reactions r_n^e and friction forces $\mathbf{r}_t^e$. The facing nodes are in contact if $r_n^e < 0$. These contact nodes are then sliding if $\|\mathbf{r}_t^e\| = -\mu r_n^e$ and sticking if $\|\mathbf{r}_\mathbf{t}^\mathbf{e}\| < -\mu r_n^e$.

4.2 Complex Eigenvalue Analysis (CEA) in case of full steady sliding

Stability analysis is only carried out in the case of full steady sliding (no sticking region) and maintained contact configuration: it is thus assumed that for each node in contact at equilibrium, bilateral contact and

sliding Coulomb friction laws apply. In order to perform the stability analysis, these laws have to be linearized. On effective contact region, the linearized forms of Eqs. (3) and (5) with the above assumptions can be written (cf. for instance [12]):

$$\begin{aligned} \Delta u_n &= 0 \\ \mathbf{r}_t &= -\mu r_n \mathbf{t} - c_b \dot{u}_b \mathbf{b} \end{aligned} \tag{16}$$

where $c_b = -\mu r_n^e / \|\dot{\mathbf{s}}_t^e\|$ is a damping term due to the linearisation of the sliding direction of the friction force and $\mathbf{b}$ is the tangential direction orthogonal to $\mathbf{t}$.

Searching a discrete solution of the form $\mathbf{U^e} + \tilde{\mathbf{U}} \exp(\lambda t)$ where $\tilde{\mathbf{U}}$ stands for the complex displacement vector corresponding to small harmonic perturbations around the equilibrium, the linearized form of equation (7) leads to a constrained non symmetric eigenvalues problem:

$$\begin{aligned} (\lambda^2 \mathbf{M} + \lambda(\mathbf{C} + \mathbf{C_b}) + \mathbf{K})\tilde{\mathbf{U}} &= (\tilde{\mathbf{P}}_\mathbf{n}^T + \mu \tilde{\mathbf{P}}_\mathbf{t}^T)\tilde{\mathbf{R}}_\mathbf{n} \\ \tilde{\mathbf{P}}_\mathbf{n}\tilde{\mathbf{U}} &= 0 \end{aligned} \tag{17}$$

where $\mathbf{C_b}$ is the damping matrix provided by the linearisation of the sliding direction of friction force [12, 14, 13] and $\tilde{\mathbf{P}}_\mathbf{n}, \tilde{\mathbf{P}}_\mathbf{t}$ are new projections matrices such that $\tilde{\mathbf{P}}_\mathbf{n}$ is the restriction of $\mathbf{P_n}$ on nodes in the effective contact region at equilibrium whereas $\tilde{\mathbf{P}}_\mathbf{t}$ is the restriction of $\mathbf{P_t}$ on components in direction $\mathbf{t}$ on nodes in the effective contact region. In stable cases, the perturbations vanish and no vibration occur. In unstable cases, Complex modes and eigenvalues of the problem are then calculated. Modes corresponding to eigenvalues with negative real part are stable. In this case, the perturbations corresponding to these modes vanish and no vibration occur. On the other hand, modes corresponding to eigenvalues with positive real part are unstable. Some perturbations corresponding to these modes tend to diverge which can lead to self-sustained vibrations. The divergence rate of a mode is notably defined as $\mathrm{Re}(\lambda)/\mathrm{Im}(\lambda)$ where $(\mathrm{Re}(\lambda), \mathrm{Im}(\lambda))$ are respectively the real and imaginary parts (pulsation) of the mode. This rate corresponds to a negative damping rate.

4.3 Reduced CEA formulations

Solving such a large non-symmetric eigenvalue problem needs model reduction. The approximation consisting in neglecting the dynamic part of the attachments modes is also tested for the stability analysis. The same technique used in section 3 is applied. The reduction is first performed with basis $\mathbf{B} = [\Phi \quad \tilde{\Phi}_{sn}]$ composed of free-interface component modes Φ and static attachment residual modes $\tilde{\Phi}_{sn}$ defined on effective contact region by:

$$\tilde{\Phi}_{sn} = \Phi_{sn} - \Phi(\Phi^T \mathbf{K} \Phi)^{-1} \Phi^T \tilde{\mathbf{P}}_\mathbf{n}^T \tag{18}$$

The dynamic effects corresponding the residual attachment modes are then neglected leading to the following constrained eigenvalue problem:

$$\begin{aligned} (\lambda^2 \Phi^T \mathbf{M} \Phi + \lambda \Phi^T (\mathbf{C} + \mathbf{C_b}) \Phi + \Phi^T \mathbf{K} \Phi)\tilde{\mathbf{q}} &= \Phi^T (\tilde{\mathbf{P}}_\mathbf{n}^T + \mu \tilde{\mathbf{P}}_\mathbf{t}^T)\tilde{\mathbf{R}}_\mathbf{n} \\ \tilde{\mathbf{P}}_\mathbf{n}\tilde{\mathbf{U}} &= \tilde{\Phi}_{sn}^T (\tilde{\mathbf{P}}_\mathbf{n}^T + \mu \tilde{\mathbf{P}}_\mathbf{t}^T)\tilde{\mathbf{R}}_\mathbf{n} + \tilde{\mathbf{P}}_\mathbf{n} \Phi \tilde{\mathbf{q}} \\ \tilde{\mathbf{P}}_\mathbf{n}\tilde{\mathbf{U}} &= \mathbf{0} \end{aligned} \tag{19}$$

where $\tilde{\mathbf{q}}$ is the generalized vector corresponding to free-interface normal modes.

From the two last lines of Eq. (19), normal reactions $\tilde{\mathbf{R}}_\mathbf{n}$ can be expressed as a function of the generalized vector $\tilde{\mathbf{q}}$:

$$\tilde{\mathbf{R}}_\mathbf{n} = -\tilde{\Phi}_{sn}^T (\tilde{\mathbf{P}}_\mathbf{n}^T + \mu \tilde{\mathbf{P}}_\mathbf{t}^T))^{-1} \tilde{\mathbf{P}}_\mathbf{n} \Phi \tilde{\mathbf{q}} \tag{20}$$

Finally, using the above expression in the reduced eigenvalue problem gives:

$$(\lambda^2 \Phi^T \mathbf{M} \Phi + \lambda \Phi^T (\mathbf{C} + \mathbf{C_b}) \Phi + \Phi^T (\mathbf{K} + \mathbf{K_c}) \Phi)\tilde{\mathbf{q}} = \mathbf{0} \tag{21}$$

where $\mathbf{K_c}$ is a non-symmetric stiffness matrix taking account the effect of the local residual flexibility of the structure due to normal and friction forces:

$$\mathbf{K_c} = (\tilde{\mathbf{P}}_\mathbf{n}^T + \mu\tilde{\mathbf{P}}_\mathbf{t}^T)(\Phi_{sn}^T(\tilde{\mathbf{P}}_\mathbf{n}^T + \mu\tilde{\mathbf{P}}_\mathbf{t}^T))^{-1}\tilde{\mathbf{P}}_\mathbf{n} \tag{22}$$

This reduction strategy consists in solving the global dynamics using free-interface normal modes and adding a local static residual stiffness controlled by matrix $\mathbf{K_c}$. This matrix plays the same role than 2-DOF Hertzian stiffness/Coulomb friction relations in the case on equivalent point contact models but is calculated by finite elements.

5 Numerical methods for non linear simulations

For the computation of the quasi-static solution (Eq. (15)) and dynamics solutions at each time step (Eq. (7)), an iterative fixed point algorithm on equivalent contact reactions and friction forces is used with a stop criterion based on forces convergence [14]. This algorithm is appropriate to the formulation of the frictional contact laws as non linear projections. The main advantage of the fixed point algorithm is that the integrator matrix remains constant at each iteration. In the simulations presented in this paper, the augmented parameters ρ_n, ρ_t are chosen as the smallest eigenvalue of the integrator matrix condensed on the contact degrees of freedom [15].

For the computation of the transient solution, the chosen time integration method is a modified θ-method. This is a first-order scheme developed by Jean [8] and appropriate to unilateral contact dynamics. It notably allows to compute quasi-inelastic shocks. The detail of the scheme with an application to friction-induced vibrations can be found for instance in Loyer's work [14].

6 Results

In this section, an application of the methodology presented in the previous sections is proposed for the case of rolling contact of a wheel and a rail with lateral creepages. The model is first described. Secondly, the model is validated in quasi-static conditions with CONTACT software. A stability analysis is then carried out. Transient calculations are finally performed with reduction and results are discussed.

6.1 Description of the model

The material behavior is assumed to be linearly elastic, isotropic and undergoing small deformations. The material data of the wheel and the rail are listed in Tab. 1.

Data	Wheel	rail
Young's modulus (GPa)	206.9	205
Poisson's ratio	0.288	0.3
Density (kg/m^3)	7800	7800

Table 1: Material data of the wheel and the rail

A vertical displacement u_{z0} is applied at the hub of the wheel. For the discretization by finite elements, compatible meshes on the interface are considered: facing nodes of the wheel and the rail in potential contact have identical tangential coordinates x and y. The potential contact area is meshed with elements of length 1 mm as shown in Fig. 2.

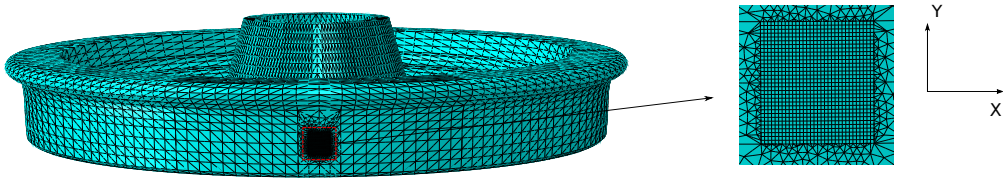

Figure 2: FE model of the wheel with fine mesh on the contact zone

6.1.1 Wheel dynamics

The dynamic behavior of the wheel is assumed to be linear and lightly damped so that a real modal basis can be used. This basis is presumed to be known in the frequency range of interest. A mode is characterized by its natural circular frequency ω_i, its vertical and lateral modal amplitudes at the contact point Φ_z and Φ_y (assumed to be normalized with respect to mass) and its structural damping factor Ξ.

The 100 first natural frequencies and corresponding free-interface modes have been calculated up to 8000 Hz. Three kinds of mode may be distinguished: the radial modes (r,m,n), the axial modes (a,m,n) and the circumferential modes (c,m,n) where n is the number of nodal diameters and m is the number of nodal circles. This classification is necessary to obtain a convergence of eigenvalues depending on the model mesh.

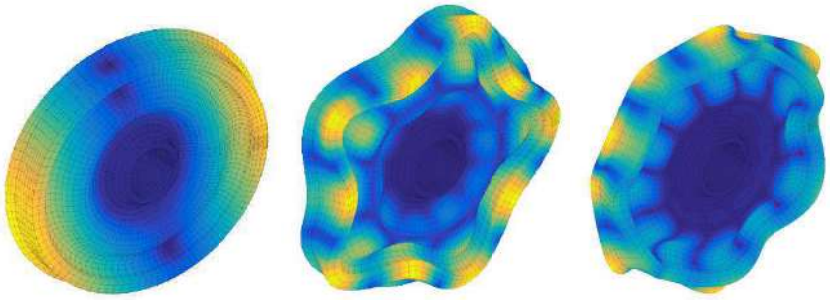

(a) (b) (c)

Figure 3: a: Mode axial of 136.4 Hz ($m = 0, n = 1$), b:Mode radial of 3281 Hz ($m = 1, n = 5$) et c: Mode axial of 3417 Hz ($m = 0, n = 6$)

Chosen modal damping factors η depend on the nodal diameters [3]:

$$\begin{cases} \eta = 10^{-3} & \text{if} \quad n = 0 \\ \eta = 10^{-2} & \text{if} \quad n = 1 \\ \eta = 10^{-4} & \text{if} \quad n \geq 2 \end{cases} \tag{23}$$

6.1.2 Rail dynamics

The rail model consists of one periodically supported rail of type UIC60 provided by ESI-Group (Fig. 4). This rail has 48m length. The space between sleepers is 60cm. However the dynamic of sleepers and ballast is neglected because of its low frequency domain.

The rail hysteresis damping is $\eta = 0.02$. The rail ends with an anechoic termination of 6 meters composed of 5 lengths $L = (0.6, 0.6, 0.6, 1.2, 3.0)$m which are associated variable structural damping $\eta = 0.1|1$ to avoid the return of waves. Pads that connect the rail and the sleepers are modeled by springs $(Kx = Ky = 36e6, Kz = 180e6)$N/m. The pad hysteresis damping is $\eta = 1$.

The dynamic response obtained by FEM is compared with the dynamic response obtained with the analytical model as Timoshenko beam [16]. The vertical mobilities at the center point between two sleepers and on

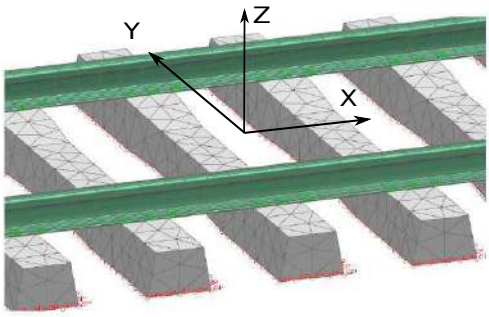

Figure 4: Rail model

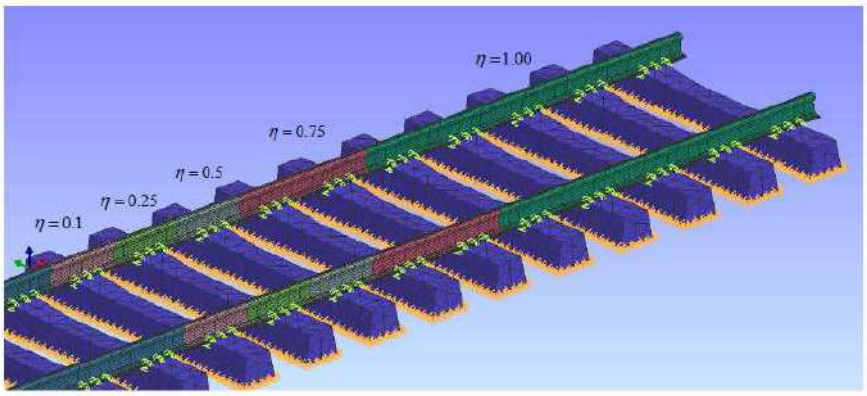

Figure 5: Rail anechoic termination

a sleeper are represented in Fig. 6. The frequencies of the peaks are close. However the amplitudes are different at the peak that associates to the distance between two sleepers. This difference results from the uniform distribution of the springs that connect the rail and the sleepers. In the Timoshenko beam, there is only a spring that connects the rail and the sleepers.

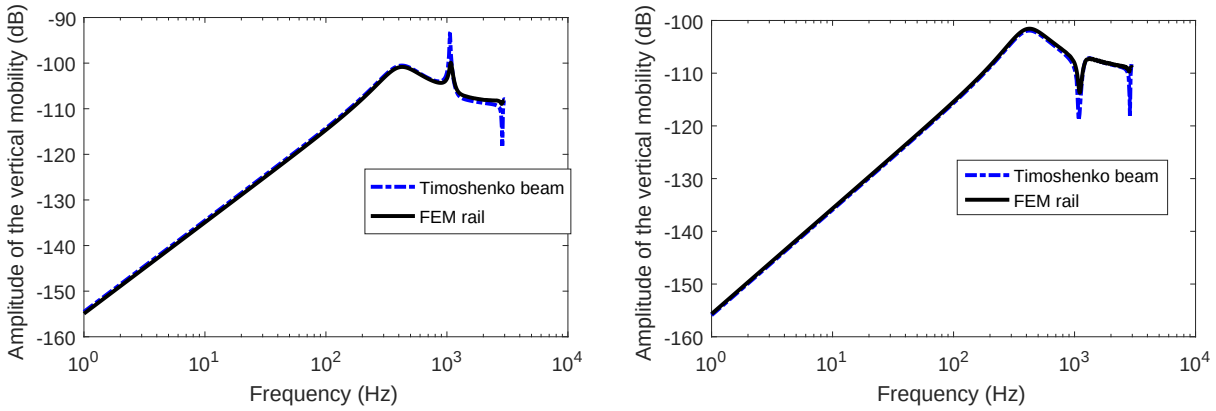

(a) between two sleepers

(b) on a sleeper

Figure 6: Vertical mobility

6.2 Quasi-static results

In this section the wheel/rail quasi-static rolling contact with lateral creepage is considered. The rolling is performed in the $-x$ direction with $V = 10$ m/s. An vertical displacement $u_{z0} = 0.35$ mm is applied leading

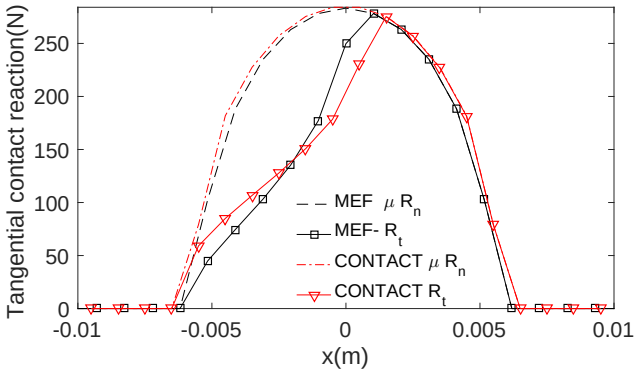

Figure 7: Quasi-static frictional stresses on a line $y = 0$ for $\Delta V_y/V = 0.2\%$ and $\mu = 0.3$

to a resultant vertical contact force of about 66 kN. A friction coefficient $\mu = 0.3$ is considered. Longitudinal and spin creepages are set to zero ($\Delta V_x = \Delta\omega_z = 0$).

For an imposed lateral creepage $\Delta V_y/V = 0.2\%$, the longitudinal distributions of the normal contact reactions and frictional reaction on the center line of the contact zone ($y = 0$) are presented in Fig. 7. As expected, a stick zone occurs at the leading edge of the contact and a slip zone occurs at the trailing edge of the contact. The comparison of the results obtained with the proposed full FE method and the results provided by CONTACT software shows a good agreement in the slip zone and some differences for the tangential stresses in the stick zone.

6.3 Stability results

Stability analysis is carried out in case of full sliding using a higher creepage $\Delta V_y/V = 1\%$. In order to solve the non symmetric eigenvalue problem, the reduction strategy presented in section 4.3 (contact static approximation) is performed. 4 unstable modes whose real parts are positive are obtained. The frequency of these unstable complex modes are 334, 918, 1670 and 3417 Hz respectively. These frequencies obtained get close to those observed experimentally. Figs. 9 to 12 show the unstable modes shape. There are 3 axial wheel modes of (2,3,4) nodal diameters and one wheel mode (a,1,6).

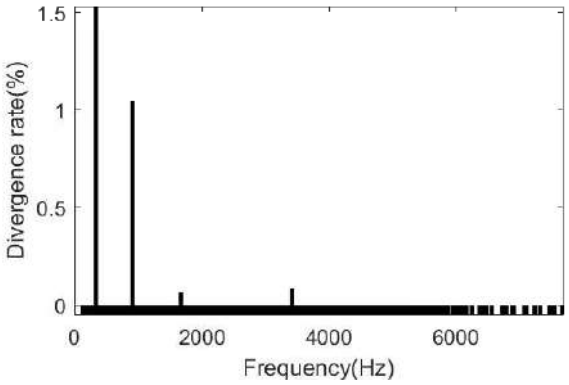

Figure 8: Divergence rate of the complex modes

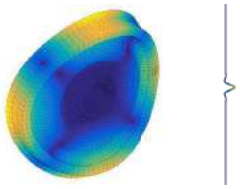

(a) Wheel (b) Rail

Figure 9: Unstable mode shape 1 (334 Hz)

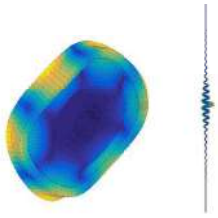

(a) Wheel (b) Rail

Figure 10: Unstable mode shape 2 (918 Hz)

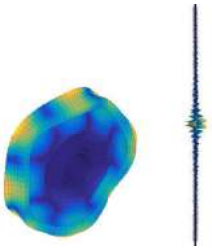

(a) Wheel (b) Rail

Figure 11: Unstable mode shape 3 (1670 Hz)

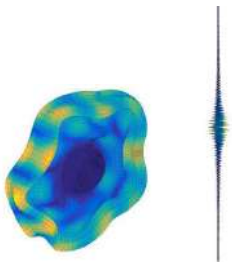

(a) Wheel (b) Rail

Figure 12: Unstable mode shape 4 (3417 Hz)

6.4 Transient results

Transient results corresponding to the unstable case founded in the previous section are determined using a numerical time integration from given initial conditions. In all the following results, the integration starts from the equilibrium i.e. the initial displacements are the displacements obtained from the quasi-static solution and the initial velocities are null. The parameters $V_x = 10$ m/s, $\mu = 0.3$ and $\Delta V_y/V = 1\%$ are used. The time step for the integration is $\Delta t = 1\mu$s.

Fig. 13a show the time series of the lateral contact resultant forces F_t. The tangential resultant force increases until a pronounced stick/slip oscillation builds up as shown in Fig. 13b. When the tangential contact resultant force is smaller than the traction bound μF_n, a transient stick zone appears at the leading edge of the effective contact region as shown in Fig. 14.

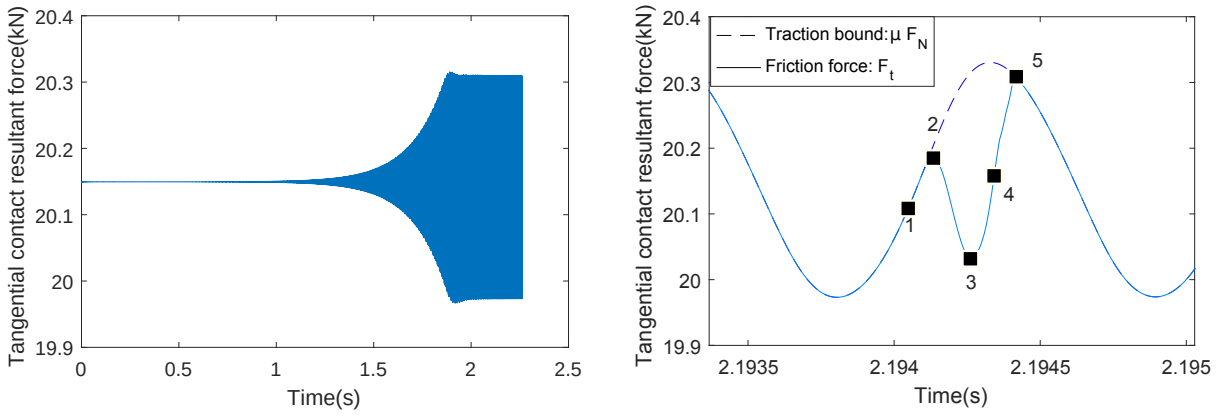

(a) Temporal evolution (b) Zoom on time series

Figure 13: Tangential contact resultant force. The status of the contact points at the time steps marked with Arabic numerals is represented Fig. 14

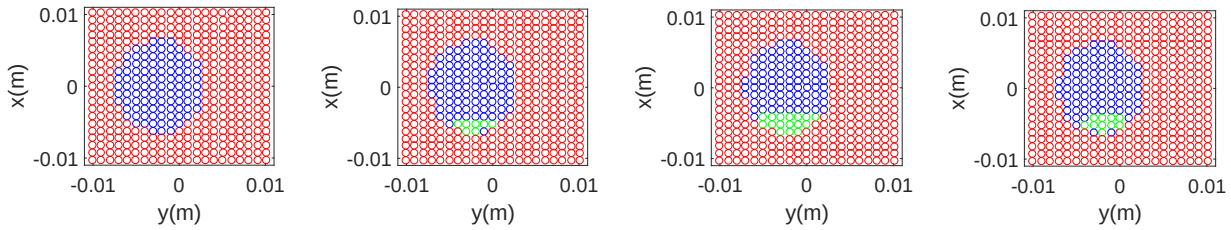

(a) 1&5 (b) 2 (c) 3 (d) 4

Figure 14: Status of nodes in the potential contact zone: no contact zone (red), slip zone (blue) and stick zone (green)

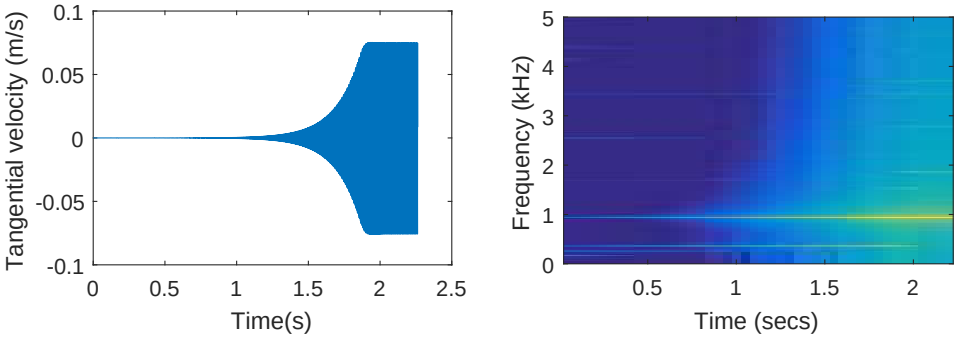

(a) Temporal evolution (b) Spectrogram (time-frequency)

Figure 15: Tangent velocity of a point outside the contact zone

The time series of the lateral velocity of a point outside the contact zone is presented in the Figure 15a. The spectrogram in Fig. 15b allows to observe which frequencies are present in the solution and when they appear. At the beginning, there are two major frequencies: 334 and 919 Hz which get very close to the natural frequencies of to the two premier unstable modes provided by stability analysis. In the stationary step where nonlinear events happen, the dominant frequency is $f_0 = 919$ Hz and its harmonic frequencies $f_k = kf_0$ appear.

7 Conclusion

In this paper, a method is presented for the modeling and analysis of the high-frequency friction-induced instabilities of wheel/rail frictional rolling contact in time and frequency domains. A full finite element formulation around the stationary position in an Eulerian reference frame is derived with a fine discretization of the contact surface combined with unilateral and Coulomb friction laws with constant friction coefficient. Both stability analysis and transient calculation are performed not only to determine unstable modes and frequencies but also to determine the amplitude and the full spectrum of vibrations.

In order to reduce the computational effort, a reduction strategy is proposed for both domains. The technique consists in simply adding a residual static contact flexibility to the free-interface normal modes when solving the frictional contact equations (contact static approximation).

The method is tested in the case of wheel/rail frictional rolling contact. The obtained results are first compared to analytical results and Kalkers theory in the quasi-static case. Application to narrow curves configuration shows that self-excited vibrations of the wheel / rail curve contact could occur due to mode coupling instability (with constant friction coefficient). The results of transient dynamics exhibit are consistent with the stability analysis and exhibit the corresponding localized stick/slip oscillations in the contact zone.

Acknowledgements

This work was carried out within the CERVIFER project backed by the ADEME organization and the Haut-de-France region. It was also supported by the LabEx CeLyA of University of Lyon, operated by the French National Research Agency (ANR-10-LABX-0060/ANR-11-IDEX-0007). The authors gratefully acknowledge the support of these institutions.

References

[1] J.Ayasse, H.Chollet, *4 Wheel–Rail Contact*, Handbook of railway vehicle dynamics, CRC Press (2006), pp. 85.

[2] JJ.Kalker, *Wheel-rail rolling contact theory*, Wear, Elsevier (1991), pp. 243-261.

[3] D.Thompson, *Railway noise and vibration: mechanisms, modelling and means of control*, W Elsevier (2008).

[4] A.Pieringer, *A numerical investigation of curve squeal in the case of constant wheel/rail friction*, Journal of Sound and Vibration, Elsevier (2014), pp. 4295-4313.

[5] J.Dahlberg, B.Alfredsson, *Transient rolling of cylindrical contacts with constant and linearly increasing applied slip*, Wear, Elsevier (2009), pp. 316-326.

[6] M.Toumi, H.Chollet, H.Yin, *Finite element analysis of the frictional wheel-rail rolling contact using explicit and implicit methods*, Wear, Elsevier (1991), pp. 243-261.

[7] K.-L.Johnson, *Contact mechanics*, Cambridge university press (1987).

[8] M.Jean, *The non-smooth contact dynamics method*, Computer methods in applied mechanics and engineering, Elsevier (1999), pp. 235-257.

[9] P.Chambrette, L.Jezequel, *Stability of a beam rubbed against a rotating disc*, European journal of mechanics. A. Solids, Elsevier (1992), pp. 107-138.

[10] M.Raous, S.Barbarin, D.Vol, *Numerical characterization and computation of dynamic instabilities for frictional contact problems*, Friction and Instabilities, Springer (2002), pp. 233-291.

[11] A.-D.Kudawoo, *Problèmes industriels de grande dimension en mécanique numérique du contact: performance, fiabilité et robustesse*, Université de Provence-Aix-Marseille I (2012).

[12] D.Brizard, O.Chiello, J.-J.Sinou, X.Lorang, *Performances of some reduced bases for the stability analysis of a disc/pads system in sliding contact*, Journal of Sound and Vibration, Elsevier (2011), pp. 703-720.

[13] X.Lorang, F.Foy-Margiocchi, Q.-S.Nguyen,Gautier, *TGV disc brake squeal*, Journal of Sound and Vibration, Elsevier (2006), pp. 735-746.

[14] A.Loyer, J.-J.Sinou, O.Chiello, X.Lorang, *Study of nonlinear behaviors and modal reductions for friction destabilized systems. Application to an elastic layer*, Journal of Sound and Vibration, Elsevier (2012), pp. 1011-1041.

[15] H.-B.Khenous, J.Pommier, Y.Renard, *Hybrid discretization of the Signorini problem with Coulomb friction. Theoretical aspects and comparison of some numerical solvers*, Applied Numerical Mathematics, Elsevier (2006), pp. 163-192.

[16] J.-F.Hamet, *Railway noise: use of the Timoshenko model in rail vibration studies*, Acta Acustica united with Acustica, S. Hirzel Verlag (1999), pp. 54-62.

[17] B.Ding, G.Squicciarini, D.J.Thompson, *Effects of rail dynamics and friction characteristics on curve squeal*, Journal of Physics: Conference Series, IOP Publishing (2016), pp. 012146.